Kinetic Study of the Competitive Growth Between θ-Al$_2$O$_3$ and α-Al$_2$O$_3$ During the Early Stages of Oxidation of β-(Ni,Pt)Al Bond Coat Systems: Effects of Low Oxygen Partial Pressure and Temperature

J.M. ALVARADO-OROZCO, R. MORALES-ESTRELLA, M.S. BOLDRICK,
G. TRAPAGA-MARTINEZ, B. GLEESON, and J. MUNOZ-SALDANA

An oxidation study of β-(Ni,Pt)Al commercial bond coat systems was carried by means of TGA analysis during isothermal treatments at temperatures from 1273 K to 1423 K (1000 °C to 1150 °C). The effect of oxygen partial pressure on their oxidation kinetics was studied and complemented by photo-stimulated luminescence spectroscopy and SEM. Pre-oxidation treatments performed on as-aluminized samples at 10^{-5} atm O$_2$ did not accelerate the θ-Al$_2$O$_3 \rightarrow$ α-Al$_2$O$_3$ transformation, even after 5 hours of oxidation relative to samples oxidized in 0.21 atm O$_2$, with the exception of the sample treated at 1273 K (1000 °C), where apparently α-Al$_2$O$_3$ nucleation started earlier for the sample treated at a low pO$_2$.

I. INTRODUCTION

HIGH-TEMPERATURE coatings have been widely used since the 1950s to protect hot-section components in gas turbine engines against oxidation and corrosion phenomena.[1–3] In general, such coatings are either diffusion or overlay.[4] Diffusion coatings have been studied extensively in recent decades, with those based on β-NiAl being the most widely used in the land, marine, and aeronautical applications.[4–7] In order to improve the resistance of β-based coatings to oxidation and hot-corrosion, the judicious addition of elements such as Pt, Pd, Rd, Ir, Cr, Hf, Si, and Y has been investigated.[8–11] Pt-modified β-NiAl systems, the focus of the present study, are diffusion coatings comprising: (1) a Ni-based superalloy as the substrate that provides mechanical strength during operation; (2) an alumina scale forming β-(Ni,Pt)Al composition that is an aluminum reservoir to sustain the alumina-scale formation; and (3) a thermally grown oxide (TGO) resulting from the β oxidation[3,12] and acting as a diffusion barrier to prevent substrate oxidation as well as to increase its hot-corrosion resistance. In the case of thermal barrier coatings (TBC) systems, the β-based coating server as bond coat to the ceramic top coat (TC) and the intrinsic failure mechanisms as defined by Evans et al.,[12] are invariably associated with detachment along the BC/TGO interface. For instance, thermal expansion mismatch between the TGO and BC can result large compressive stresses (3 to 5 GPa) in the TGO layer during cooling.[13–16] In order to extend the service lives of TBC systems and β-NiAl coatings in general, the TGO should: (1) be α-Al$_2$O$_3$ in structure with the largest possible grain size; (2) have present a uniform columnar morphology along β-coatings surface; (3) have good adhesion between the BC and TC; and (4) be slow growing.[17–19] Rybicki and Smialek[20] and separately Brumm and Grabke[21] showed that oxidation of the intermetallic β-NiAl exhibits two polymorphic transitions (γ-Al$_2$O$_3 \rightarrow \theta$-Al$_2$O$_3 \rightarrow \alpha$-Al$_2$O$_3$) before reaching the stable α-Al$_2$O$_3$ structure. The process to establish a stable α-Al$_2$O$_3$ scale may involve several stages of nucleation and competitive growth depending of the oxidation conditions. For instance, Brumm and Grabke[21] also showed that at 1148 K (875 °C), γ-Al$_2$O$_3$ is the controlling phase from about 4 to 10 hours. A subsequent transition period of nucleation and competitive growth of θ-Al$_2$O$_3$ are observed with the continuous increase of the parabolic rate constant from about 10 to 16 hours, followed for a θ-Al$_2$O$_3$ controlling regime. However, during the early stages of oxidation (below 4 hours for this example), additional transitions (and, therefore, differences in instantaneous growth rate) can be expected due to different factors including the heating procedure, surface preparation, and specimen handling. These factors can affect the interfacial-reaction steps associated with mass at the gas/scale and/or scale/alloy interfaces, growth of transient oxides (e.g., NiAl$_2$O$_4$), etc.

Transformation to the stable α-Al$_2$O$_3$ is accompanied by a volume decrease of the lattice unit cell. For

J.M. ALVARADO-OROZCO, Research Assistant, and B. GLEESON, Department Chairman, are with the Mechanical Engineering and Materials Science Department, University of Pittsburgh, Pittsburgh, PA, 15261. R. MORALES-ESTRELLA, Professor, is with the Instituto de Investigaciones Metalurgicas, UMSHN, Edificio "U", C.U., 58060 Morelia, Michoacan, Mexico. M.S. BOLDRICK, Researcher, G. TRAPAGA-MARTINEZ, Principal, and J. MUNOZ-SALDANA, Professor, are with the Centro de Investigacion y de Estudios Avanzados del IPN, Unidad Querétaro, 76230 Querétaro, Mexico. Contact e-mail: jmunoz@qro.cinvestav.mx
Manuscript submitted April 27, 2014.
Article published online December 3, 2014.

example, the volume change associated with the $\theta\text{-Al}_2\text{O}_3 \rightarrow \alpha\text{-Al}_2\text{O}_3$ transition is a ~8 pct, reduction which can lead to defects and thermal stresses in the β/TGO interface that may promote early failure.[22]

It is important to emphasize that the deposition process of the well-know TBC systems with β-(Ni,Pt)Al bond coats includes stages that can influence the BC behavior during service, and, therefore, the TBC system's lifetime. These processes include electrolytic Pt plating[23] (*i.e.*, sulfur impurities), heat treatments and the aluminizing process,[5,9] surface preparation (*i.e.*, grit-blasting after the aluminizing), and pre-oxidation treatments[17,18,24–28] (*i.e.*, with the variables being oxygen partial pressure, temperature, heating rate, time) prior to TC deposition onto the BC surface. Results of the effect of oxygen partial pressure (p_{O_2}) and temperature on the oxidation behavior of as-aluminized β-(Ni,Pt)Al coatings during isothermal (pre-oxidation) treatments are presented in this paper. These results are part of a long study on early stage TGO formation in TBC systems.[29]

Tolpygo and Clarke[18] demonstrated, by way of thermal cycling tests at 1423 K (1150 °C) that pre-oxidation treatments in air of β-(Ni,Pt)Al BC systems to form a scale of $\alpha\text{-Al}_2\text{O}_3$ TGO prior to TC deposition can improve time to failure by up to a factor of three. At around the same time, Spitsberg and More[17] reported the effect of TGO microstructure on the durability of TBC systems with β-(Ni,Pt)Al BCs. They found that BC pre-oxidation treatment, when done under specific oxygen partial pressures, can result in greater than a factor of two improvements in TBC lifetime as compared with systems having a non-treated BC. It was concluded by these authors that pre-oxidation treatments at low p_{O_2} reduce the steady-state TGO growth rate and, therefore, the growth stress in the TGO.

Moreover, it was also inferred that a direct relation exists between the TCBs lifetime and the $\alpha\text{-Al}_2\text{O}_3$ TGO grain size. However, the optimum pre-oxidation parameters (*i.e.*, p_{O_2}, time, and temperature) were not reported in that study.

Even though the effects of pre-oxidation been considered, there remains a lack of information concerning the effects of the temperature, p_{O_2}, surface preparation, and time on the competitive growth between $\theta\text{-Al}_2\text{O}_3$ and α-Al_2O_3 during the early stages of oxidation (*i.e.*, $t < 5$ hours), which is important for optimizing the subsequent TGO growth. Thus, the specific aim of this study was to systematically determine the effects of the temperature and oxygen partial pressure on the oxide growth to the better understanding of $\theta\text{-Al}_2\text{O}_3 \rightarrow \alpha\text{-Al}_2\text{O}_3$ phase transition in order to optimize the subsequent TGO growth of commercial as-aluminized β-(Ni,Pt)Al BC systems during oxidation treatments.

II. EXPERIMENTAL PROCEDURES

A. *Sample Preparation*

The samples used in this work were provided by GE Aviation (Evendale, OH) as rectangular specimens (1.8 × 1.2 × 0.15 cm), each weighing about 2.9 g. Bond coats were produced by electroplating a thin layer of Pt onto Rene N5 single-crystal Ni-based superalloy substrates. A heat treatment was subsequently performed to diffuse Pt into the superalloy, followed by a vapor phase aluminizing (VPA) process. After a second heat treatment the desired β-(Ni,Pt)Al phase was achieved. The resulting bond coat was a bilayer structure consisting of a ~50 μm thick β-(Ni,Pt)Al and a ~20 μm thick inter-diffusion zone (IDZ) as shown in Figure 1. As indicate in Figure 1(c) the coating surface had a root-mean-

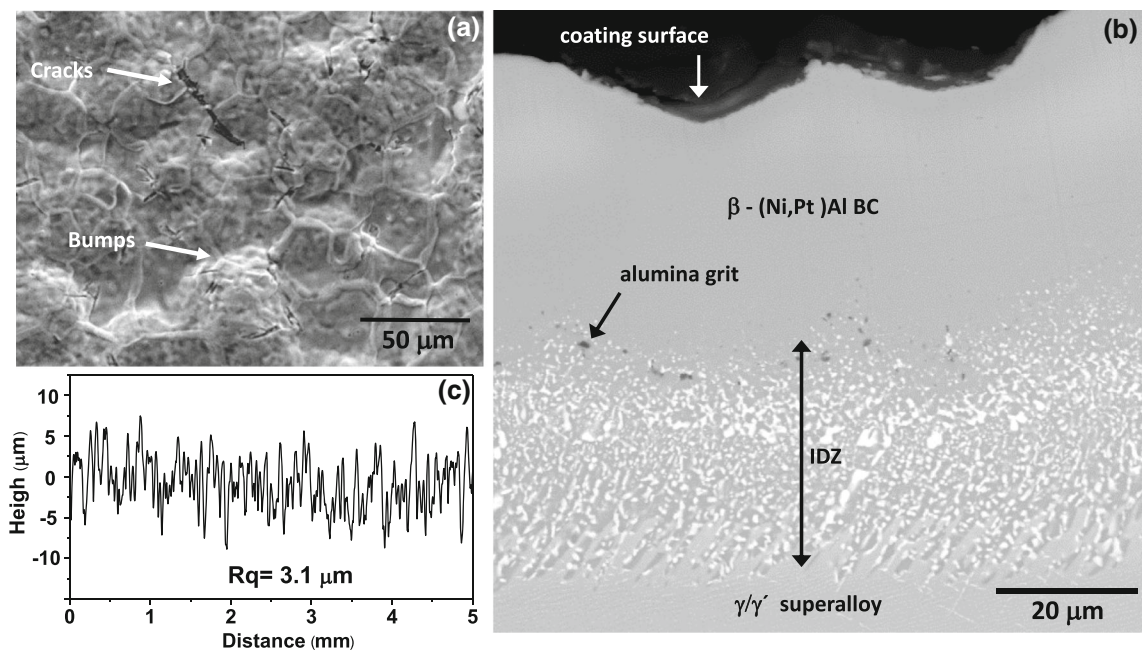Fig. 1—As-coated β-(Ni,Pt)Al BC system morphology: (*a*) surface view, (*b*) cross-sectional, and (*c*) the root mean square roughness (Rq).

Sample	Weight Percent											
	Cr	Co	Mo	Re	W	Al	Ti	Ta	Hf	Pt	Y	Ni
Nominal ReneN5*	7.0	8.0	2.0	3.0	5.0	6.2	—	7.0	0.2	—	0.01	bal.
As-received ReneN5**	6.19	8.27	1.39	3.23	5.03	6.37	0.01	6.93	0.15	—	—	bal.
As-coated β-(Ni,Pt)Al BC***	0.80	2.66	0.045	—	0.01	24.91	—	0.28	—	31.86	—	bal.

*Ref. [3].
**Measured by ICP-AES.
***Measured by EPMA.

square surface roughness (Rq) of 2.03 ± 0.29 μm as measured using a Mitutoyo Surftest SJ-201P profilometer.

The nominal compositions of the substrate and BC were determined using inductively coupled plasma atomic emission spectroscopy (ICP-AES, Perkin Elmer Optima DV4300) and an electron probe microanalyzer (EPMA, JEOL 8900 WD/ED), respectively. The results are summarized in Table I.

All samples were ultrasonically cleaned by sequentially using xylene, acetone, methanol–water (1:1), and deionized water for 15 minutes each to remove surface contamination prior to oxidation treatments.

B. Oxidation Exposures

Thermogravimetric analyses (TGA) were performed using a Setaram Setsys Evolution 16/18 thermobalance, which had an accuracy of ± 0.03 μg. The mass changes during the TGA experiments were recorded at 5 seconds intervals. A given test sample was hung from one end of the beam balance using a 0.4 mm diameter Pt/30 pctRh wire and positioned—at room temperature- in the hot-zone region of the vertical furnace. To minimize any perturbation resulting from gas flow, buoyancy, drag forces, or sample oxidation before reaching the test temperature, the heating cycle was programmed as follows: (1) evacuation of the sample chamber to less than 10 Pa; (2) heating to the reaction temperature at a maximum rate of 50 K (50 °C)/min under the same vacuum conditions; (3) back filling the chamber with working gas to atmospheric pressure using a flow rate of 200 mL/min; (4) fixing the flow of the working gas to 20 mL/min; and finally (5) cooling the furnace chamber to room temperature at a maximum rate of 50 K (50 °C)/min with a gas flow rate of 0.3 mL/min. In order to evaluate the effect of p_{O_2} on the β-(Ni,Pt)Al BC oxidation kinetics, two different conditions were used: dry air with $p_{O_2} = 0.21$ atm and argon with $p_{O_2} = 10^{-5}$ atm in the range from 1173 K to 1473 K (900 °C to 1200 °C).

C. Characterizations

The structural characterization of the TGO was monitored after each isothermal exposure (5 hours) by photo-stimulated luminescence spectroscopy (PSLS) using a micro-Raman mapping spectrometer (Renishaw InVia) connected to a Leica microscope equipped with a 532 nm line-focus laser. A 5× microscope objective was

used to focus the ~4 μm spot-sized laser beam and to collect the scattered light. The laser power at the sample was 5 mW, and the acquisition time for each spectrum was in the 0.5 to 2.0 seconds range. PSLS spectra were obtained by mapping the sample surface over a ~0.09 μm^2 area with a pitch size of 10 μm. The laser power at the sample was 5 mW, and the acquisition time for each spectrum was in the 0.5 to 2.0 seconds range. The PSLS technique is based on photon emission from Cr^{3+} ions, a typical impurity incorporated in the crystal structure of Al_2O_3 formed on alumina coatings.[16,30,31] Once illuminated, the Cr^{3+} ions emit fluorescent radiation due to radioactive decay of the excited electrons to the ground state.[32] The identification of the alumina phases is done on the basis of the well-characterized frequencies of the α-Al_2O_3 and θ-Al_2O_3.[16] Details about the PSLS spectra analysis can be found in Reference 33. The microstructure of the TGO was characterized using field emission scanning electron microscopy (Jeol JSM7401F FEG-SEM).

III. RESULTS

The plots in Figure 2(a) compare the net mass-gain (Δm) vs the square root of time ($t^{0.5}$) during isothermal oxidation of as-aluminized β-(Ni,Pt)Al coatings samples for 5 hours at the two different oxygen partial pressures of 10^{-5} and 0.21 atm O_2, and over the temperature range 1273 K to 1423 K (1000 °C to 1150 °C).

The TGA plot for the sample exposed at 1373 K (1100 °C) and 0.21 atm O_2 is not included because atypical noise during the test was observed. For oxidations in 10^{-5} atm O_2, the rate of mass gain increase of 1273 K to 1373 K (1000 °C to 1100 °C), but then abruptly decreased at 1423 K (1150 °C); whereas only an increase was observed from 1273 K to 1473 K (1000 °C to 1150 °C) for the samples exposed in 0.21 atm O_2. All the plots exhibit deviations from the straight line expected for the classic parabolic model to describe the growth of a diffusion-controlled scale, i.e.,

$$\Delta m = k_p t^{0.5}, \qquad [1]$$

where k_p is the parabolic rate constant.[34,35] The observed deviations from a constant k_p may be associated with dynamic effects such as grain-boundary diffusion (i.e., TGO grain growth), simultaneous reaction steps (i.e., interfacial-reaction steps associated with mass or defect transfer at the gas/scale and/or scale/
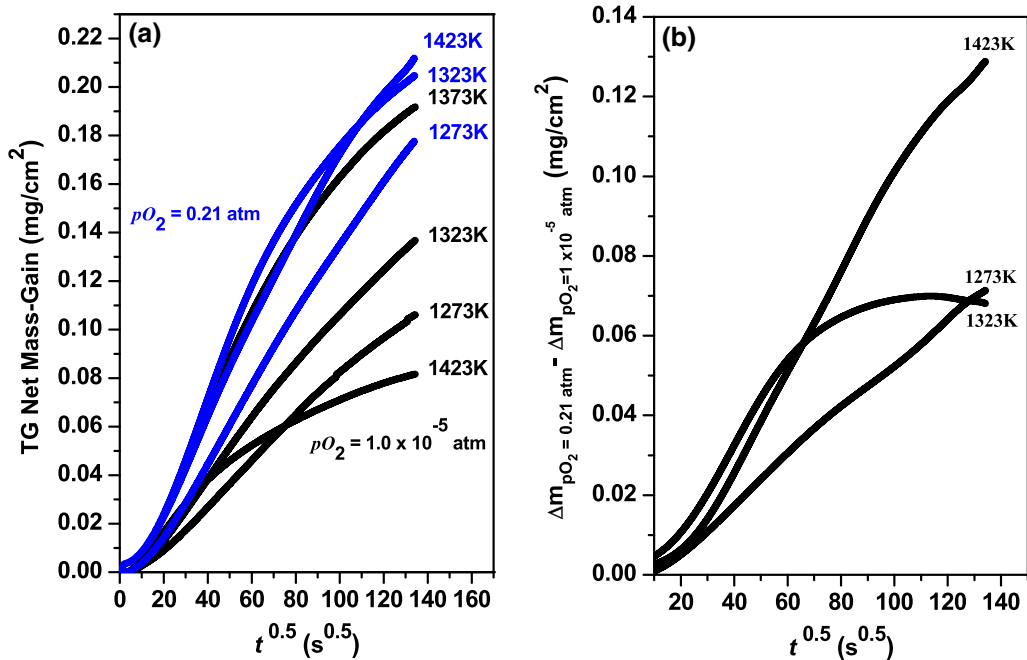
Fig. 2—(*a*) Δm vs $t^{0.5}$ curves showing the early stage (up to 5 h) oxidation behavior of as-aluminized β-(Ni,Pt)Al BC's and (*b*) the net mass-gain difference between the samples oxidized at p_{O_2} = 0.21 atm and p_{O_2} = 10^{-5} atm.
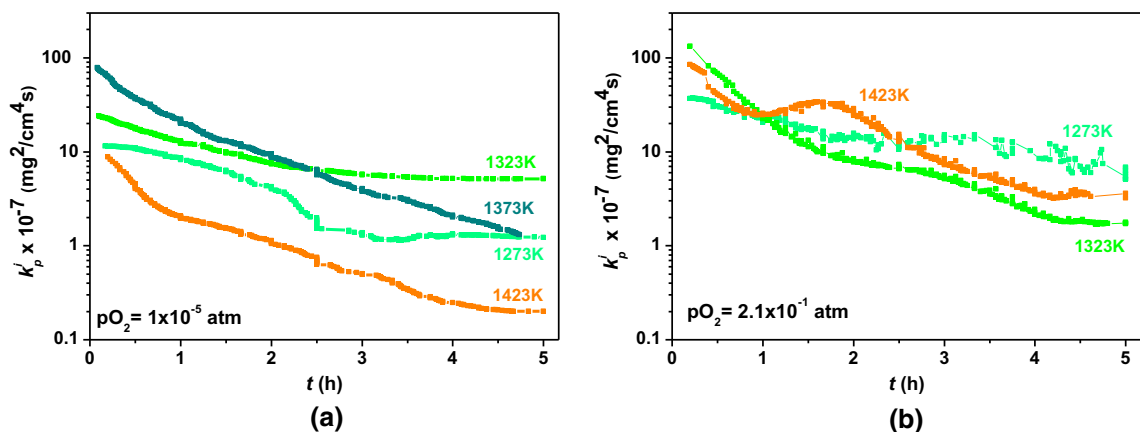

Fig. 3—Log k_p^i plotted as a function of time for as-aluminized β-(Ni,Pt)Al BC system samples during isothermal oxidation at different temperatures and oxygen partial pressures: (*a*) p_{O_2} = 10^{-5} atm and (*b*) p_{O_2} = 0.21 atm.

alloy interfaces[36]), and/or the polymorphism of Al_2O_3 and associated transformations within the TGO. Brumm and Grabke[21] investigated the oxidation kinetics of NiAl and NiAl-Cr alloys. The oxidation kinetics showed two phase transformations from γ-Al_2O_3 $\rightarrow$ θ-Al_2O_3 $\rightarrow$ α-Al_2O_3. The $\gamma \rightarrow \theta$ transformations lead to a small increase in the k_p, whereas that the $\theta \rightarrow \alpha$ leads to a strong decrease of parabolic rate constant, k_p, over two orders of magnitude. Based on the different growth kinetics of the alumina phases, a deviation from the classic parabolic model is expected if an alumina phase transformation is taking place during the oxidation exposure.

Figure 2(b) shows the differences between the instantaneous net mass-gain in 0.21 atm O_2 and that measured in 10^{-5} atm O_2 at 1273 K, 1323 K, and 1423 K

(1000 °C, 1050 °C, and 1150 °C). A marked deviation is shown for the mass-gain difference at 1323 K (1050 °C), which suggest a significant change in the oxidation behavior at the two p_{O_2} levels.

The instantaneous parabolic rate constant, k_p^i, was estimated using the data presented in Figure 2(a) and using a local fitting procedure proposed by Monceau and Pieraggi[36] for the general parabolic law:

$$t = A + B\Delta m + C\Delta m^2,\qquad [2]$$

where the coefficients A and B can be related to different kinetic parameters and C is directly related to the inverse of k_p. Figures 3(a) and (b) show the time dependence of k_p^i. As seen in this figure, all samples reached a steady state after almost 4 hours of exposure, except for the
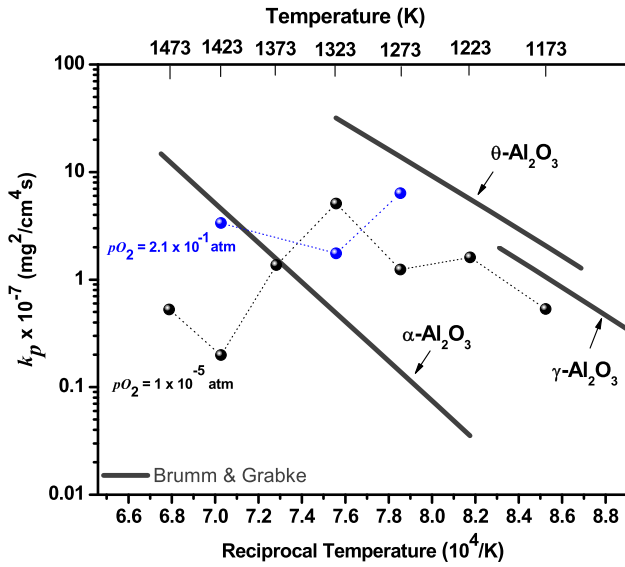
Fig. 4—Arrhenius plot showing the k_p values of as-aluminized β-(Ni,Pt)Al BC systems after 5 h of isothermal oxidation at different temperatures and oxygen partial pressures: (a) $p_{O_2} = 10^{-5}$ atm and (b) $p_{O_2} = 0.21$ atm. Bold lines correspond to the γ-, θ-, and α-Al$_2$O$_3$ lines reported by Brumm and Grabke[21].
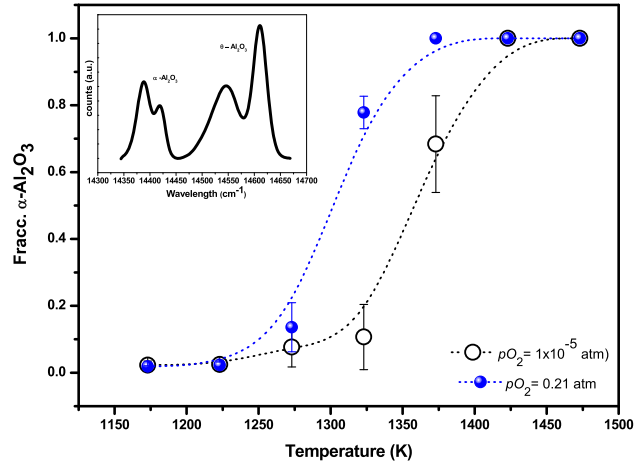

Fig. 5—Comparison of the θ-Al$_2$O$_3 \rightarrow \alpha$-Al$_2$O$_3$ transformation as a function of temperature after 5 h of isothermal oxidation of β-(Ni,Pt)Al BC's with (a) $p_{O_2} = 10^{-5}$ atm and (b) $p_{O_2} = 0.21$ atm These results were obtained by image analysis of PSLS mappings. A typical PSLS spectrum for a TGO composed of both α- and θ-Al$_2$O$_3$ phases is also shown.

sample exposed at 1373 K (1100 °C) in 10^{-5} atm O$_2$ for which k_p^i is still decreasing after 4.5 hours of exposure.

Figure 4 summarizes in an Arrhenius plot the parabolic rate constants estimated after 5 hours ex, with the data reported by Brumm and Grabke[21] for NiAl alloy oxidation included to provide a frame of reference. These results will be analyzed and discussed in the next section; however, at this point it can be sated that a significant difference is observed in comparison with the reference system, especially at low p_{O_2}.

In order to determine if the observed deviations are related to the polymorphic transformation of the Al$_2$O$_3$, a systematic structural characterization by PSLS was carried out on the TGO surface of all samples. Figure 5 compares a semiquantitative estimation of the α-Al$_2$O$_3$ fraction as a function of temperature for a fixed exposure of 5 hours for all the tested conditions.

A sigmoidal behavior is observed for both p_{O_2} conditions with a more extensive θ-Al$_2$O$_3 \rightarrow \alpha$-Al$_2$O$_3$ transformation for the samples oxidized in 0.21 atm O$_2$ from 1273 K to 1373 K (1000 °C to 1100 °C), reaching the 100 pct α-Al$_2$O$_3$ plateau at 1373 K and 1423 K (1100 °C to 1150 °C) for 0.21 and 10^{-5} atm O$_2$, respectively. The results in Figure 5, suggest that at 1173 K to 1323 K (900 °C to 1050 °C) in 10^{-5} atm O$_2$ the TGO growth kinetics during the first 5 hours of oxidation are mainly controlled by θ-Al$_2$O$_3$ (γ-Al$_2$O$_3$ signal was not observed during PSLS analysis).

IV. DISCUSSION

Simultaneous comparisons of the data presented in Figures 2, 3, 4, and 5 are necessary to provide a better understanding of the θ-Al$_2$O$_3 \rightarrow \alpha$-Al$_2$O$_3$ transformation process. Three different exposures temperatures [1273 K, 1323 K, and 1423 K (1000 °C, 1050 °C, and 1150 °C)] are selected for detailed discussion in the following.

A. Exposures at 1273 K (1000 °C)

It can be assumed that θ-Al$_2$O$_3$ was the kinetically controlling phase at both oxygen potentials, at 1273 K (1000 °C), since α-Al$_2$O$_3$ fractions at 0.2 and 1×10^{-5} atm O$_2$ were about 13 and 7.5 pct, respectively, after 5 hours of oxidation (see Figure 5). This assumption is in agreement with the time evolution of the k_p^i shown in Figure 3, where a stable growth rate constant was established for both atmospheric conditions after 2.5 hours of exposure.

Since θ-Al$_2$O$_3$ can be modeled as a p-type oxide[37–39] and Al vacancies (V_{Al}''') predominate in its structure according to following the reaction (using the Kröger–Vink notation[40]):

$$O_2 = 2O_O^X + \frac{4}{3}V_{Al}''' + 4h^\cdot,$$ [3]
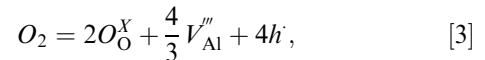
where O_O^X represents an oxygen atom in an oxygen site of Al$_2$O$_3$ and $h^\cdot$ represents an electron hole in valence band. By invoking the law of mass action and the constraint of electrical neutrality, $[h^\cdot] = 3[V_{Al}''']$, the aluminum vacancy concentration is found to be given as

$$[V_{Al}'''] = \left(\frac{K_3}{81}\right)^{3/16} p_{O_2}^{3/16}$$ [4]

Inasmuch as $[V_{Al}''']$ is proportional to k_p, it can be shown that, in accordance with Wagner's theory,[41]

$$k_p = \int_{p_{O_2}'}^{p_{O_2}''} C_1 p_{O_2}^{3/16} d\ln p_{O_2},$$ [5]

where p_{O_2}'' and p_{O_2}' represent the oxygen partial pressure at the gas-scale and metal-scale interfaces, respectively.

Following the discussion above, the θ-Al$_2$O$_3$ parabolic growth rate constant, k_p^θ, will be directly proportional to the external p_{O_2}, and therefore, a reduced rate of θ-Al$_2$O$_3$ growth is expected at low p_{O_2}. Given that $p''_{O_2} \gg p'_{O_2}$, it can be approximated

$$k_p \sim C_1 \left(p''_{O_2} \right)^{3/16} \qquad [6]$$

Based on this, the differences in net-mass gain observed at 1273 K (1000 °C) (Figure 2) should be mainly due to the decrease in the difference in environmental p_{O_2}, *i.e.*, 0.21 *vs* 10^{-5} atm O$_2$. In order to verify this effect, the following comparison can be done:

$$\frac{[k_p]_{0.21\,atm}}{[k_p]_{1\times10^{-5}\,atm}} = \frac{\left[p''^{3/16}_{O_2} \right]_{0.21\,atm}}{\left[p''^{3/16}_{O_2} \right]_{1\times10^{-5}\,atm}} = 6.46 \qquad [7]$$

k_p values can also be directly read from Figure 3, *i.e.*, $[k_p]_{0.21\,atm} = 7.2 \times 10^{-7}$ mg^2/cm^4 s and $[k_p]_{1\times10^{-5}\,atm} = 1.2 \times 10^{-7}$ mg^2/cm^4 s. Thus, experimentally it is found

$$\frac{[k_p]_{0.21\,atm}}{[k_p]_{1x10^{-5}\,atm}} = 6$$

This k_p ratio is in reasonable agreement with the expected value of 6.46 value to the extent that it can be concluded that the observed net-mass gains are in accordance with θ-Al$_2$O$_3$ growth which, in then is in accordance with Eq. [6].

B. *Exposures at 1323 K (1050 °C)*

A distinct difference in the fraction of α-Al$_2$O$_3$ was observed for the samples oxidized at 1323 K (1050 °C). Specifically, the sample exposed to 0.21 atm O$_2$ showed a higher α-Al$_2$O$_3$ volume fraction (~78 pct) in comparison with the sample exposed to 10^{-5} atm O$_2$ (~11 pct) after 5 hours of oxidation (see Figure 5). Moreover, the sample exposed to 0.21 atm O$_2$ always showed a higher net-mas gain with respect to the 10^{-5} atm O$_2$, as shown in Figure 6(a). At first glance, these results might seem contradictory, given that low p_{O_2} conditions slow θ-Al$_2$O$_3$ growth (Eq. [6]), and since that θ-Al$_2$O$_3$ growth rate is reported to be approximately two orders of magnitude higher than α-Al$_2$O$_3$ at 1323 K (1050 °C).[21] However, when the net mass-gain difference between these two conditions is estimated (Figure 2(b)), some answers can be realized in order to support the PSLS observations. The net mass-gain difference at 1323 K (1050 °C) shows how the mass gain in 0.21 atm O$_2$ decreases with the time to values where

$$\Delta m_{pO_2=0.21\,atm} < \Delta m_{pO_2=1\times10^{-5}\,atm}$$

for times greater than about 3 hours (~104 s$^{0.5}$), suggesting that a slower-growing phase (*i.e.*, α-Al$_2$O$_3$) is starting to control the oxidation kinetics.

In order to understand the possible nature of this apparently faster transformation at 1323 K (1050 °C), the following discussion can be done. It will be assumed that the θ-Al$_2$O$_3 \rightarrow \alpha$-Al$_2$O$_3$ transformation rate follows a basic diffusional nucleation model of the form[42]
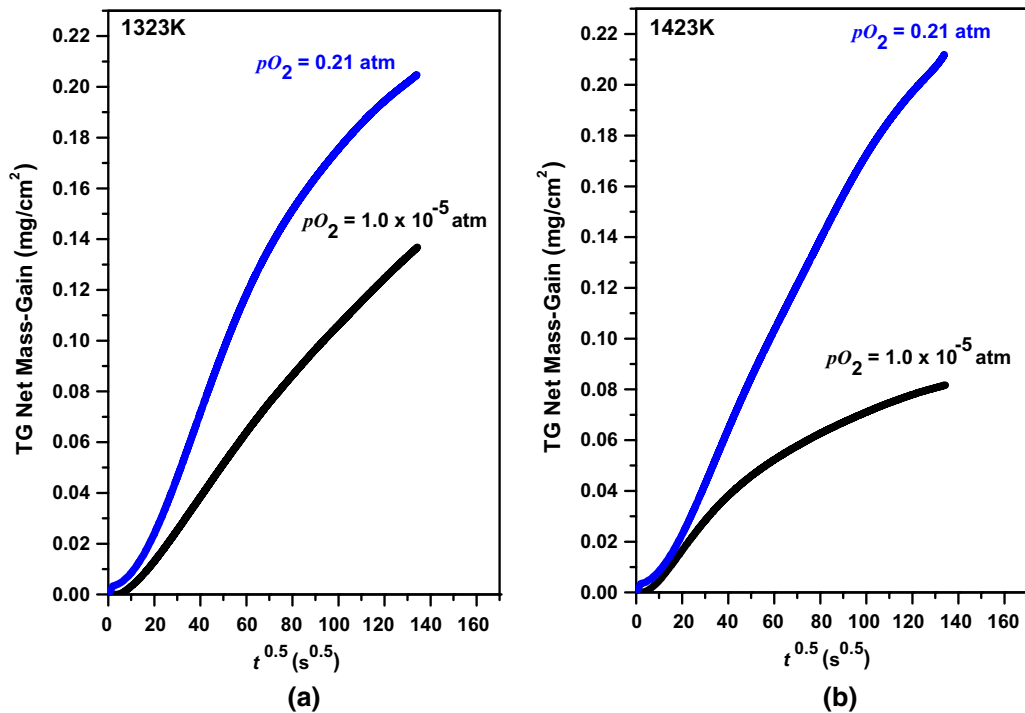

Fig. 6—Δm *vs* $t^{0.5}$ curves showing the effect of the p_{O_2} on the oxidation behavior of as-aluminized β-(Ni,Pt)Al BĆs after 5 h of oxidation: (*a*) 1323 K (1050 °C) and (*b*) 1423 K (1150 °C).

$$J^* = ZN \exp\left(-\frac{\Delta G^*}{kT}\right)\beta^* \quad \text{(nuclei/m}^3\text{s)}, \qquad [8]$$

where J^* is the nucleation rate, Z is the Zeldovich non-equilibrium factor (~0.1), N is number of sites available for nucleation per unit of volume, ΔG^* is the standard free energy change per critical nucleus to achieve the transformation and is directly proportional to the cube of the interfacial energy ($\Delta G^* \propto \gamma^3$) and is also strongly temperature dependent, and β^* is a transport coefficient related with the frequency at which single atoms join the nuclei and in accordance with Arrhenius. Thus, Eq. [8] can be rewritten as

$$J^* = Z\omega N \exp\left(-\frac{\Delta G^*}{kT}\right)\exp\left(-\frac{\Delta G_m}{kT}\right) \quad \text{(nuclei/m}^3\text{s)},$$
$$[9]$$

where ΔG_m is the activation energy for atomic migration and ω is a factor that includes the area of the critical nucleus, as well as the vibrational frequency of the atoms forming the nucleus.

Inasmuch as the Al vacancy concentration in θ-Al_2O_3 is a function of the p_{O_2} based on Eqs. [4], it is deduced that that $[V_{Al'''}]_{pO_2=0.21\,atm} > [V_{Al'''}]_{pO_2=1\times10^{-5}\,atm}$ at the gas/scale interface. Since k_p is proportional to $[V_{Al'''}]$, a greater inward flux of $[V_{Al'''}]$ and, therefore, a greater outward flux of Al^{3+} from the alloy is expected for the sample oxidized in 0.21 atm O_2. The more rapid growth of θ-Al_2O_3 in 0.21 atm O_2 contribute to a more severe depletion of the BC aluminum. The p-type nature of the θ-Al_2O_3 means that the new oxide is formed at the gas/θ-Al_2O_3 interface and vacancies diffuse inward through the growing oxide and accumulate scale/alloy interface promoting the nucleation and subsequent growth of interfacial voids. On the other hand, the mass transfer of Al in the β-NiAl BC occurs *via* vacancy diffusion. Brumm and Grabke[43] have been systematically studied the void formation for different β-NiAl alloy compositions and they found that void formation increase with increasing [Ni]/[Al] ratio due to vacancy injection (Kirkendall effect) at scale/alloy interface. Pint[44] also studied the interfacial void formation of Al_2O_3 forming alloys showing small voids (20 to 200 nm) have been observed even for the adherent reactive-element-doped scales. It was also established that when the voids remains small (20 to 50 nm) they can have a little effect on the scale adhesion, and this can even be incorporated into the growing scale if new oxide forms, primary at the scale/oxide interface. Moreover, Bagwell *et al.*[42] studied the nucleation of α-Al_2O_3 from θ-Al_2O_3, concluding that a critical θ-Al_2O_3 is not a prerequisite for α-Al_2O_3 nucleation but is a result of the incubation time to produce α-Al_2O_3 nuclei by diffusional nucleation with a subsequent rapid growth of the α-Al_2O_3 nuclei due to the heat generated during the exothermic θ-$Al_2O_3 \rightarrow \alpha$-$Al_2O_3$ transformation resulting in abnormal large initial α-Al_2O_3 grains (100 to 1000 nm). Since α-Al_2O_3 is the only stable phase of alumina, it will be expected that any process increasing the diffusive transport in the formation of the α-Al_2O_3 nuclei in Eq. [8] will be beneficial to the transformation. β^* is a term repre-

senting the frequency that a critical nucleus can receive an atom which depend on the surface area and the diffusion rate of atoms crossing the unstable nucleus. Based on this, it is proposed in the present work that β^* should be a directly proportional to Al vacancy concentration

$$\beta^* = \omega \exp\left(-\frac{\Delta G_m}{kT}\right) \propto [V_{Al'''}] \qquad [10]$$

Taking the previous discussion into account, a higher concentration of defects is anticipated at the θ-Al_2O_3/alloy interface for the sample oxidized in 0.21 atm O_2 due to higher rate of the vacancy condensation and void formation at this interface, making this interface suitable for α-Al_2O_3 nucleation, since a greater decrease of ΔG_m will increase its nucleation rate.

Based on Figure 7 and taking into account the discussion above, three different regimes may be proposed for the sample oxidized at 1323 K (1050 °C) and 0.21 atm O_2 (blue curve) using the sample oxidized in 10^{-5} atm O_2 as a framework for comparison, and assuming that θ-Al_2O_3 was the controlling phase at $t < 5$ hours under this conditions.

Regime I corresponds to $0 < t < 1.5$ hours, where the relatively high k_p^i corresponds to θ-Al_2O_3 growth. *Regime II*, for about $1.5 < t < 3$ hours, where the k_p^i for the sample exposed to 0.21 atm O_2 is almost equal to the k_p^i at 10^{-5} atm O_2 where θ-Al_2O_3 is controlling the TGO growth due to the still incipient α-Al_2O_3 nucleation. *Region III*, for about $t > 3$ hours, the α-Al_2O_3 nucleation rate for the sample tested in 0.21 atm O_2 is faster than sample oxidized in 10^{-5} atm O_2.

C. Exposures at 1423 K (1150 °C)

For the samples oxidized at 1423 K (1150 °C) only α-Al_2O_3 signal was by PSLS after 5 hours of oxidation (see Figure 5). However, this was the temperature that showed the greatest net mass-gain difference (see Figures 2(b) and 6(b)), which suggests that a different structural evolution of the TGO took place, even when
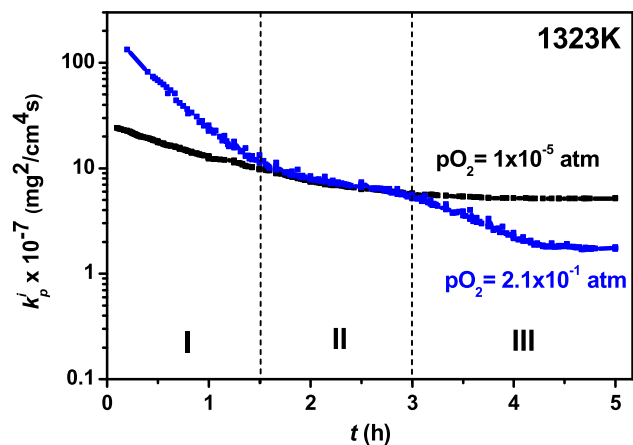
Fig. 7—Comparison of the k_p^i values *vs* time for the as-aluminized β-(Ni,Pt)Al BC samples isothermal oxidized at 1323 K (1050 °C) in a $p_{O_2} = 1 \times 10^{-5}$ atm (black curve) and $p_{O_2} = 0.21$ atm (blue curve) (Color figure online).
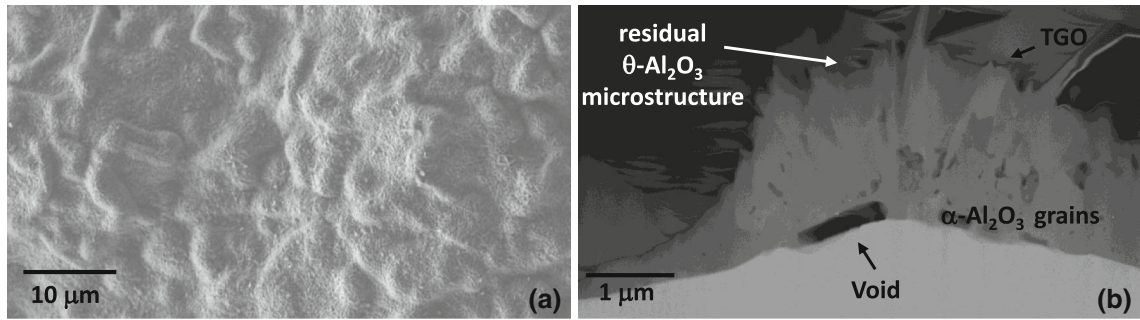
Fig. 8—Thermally grown oxide morphology after 5 h of isothermal oxidation with a $p_{O_2} = 1 \times 10^{-5}$ atm. Surface morphology (*a*) and cross-section (*b*) view of the samples oxidized at 1423 K (1150 °C).

α-Al$_2$O$_3$ was the only phase present after 5 hours of exposure. At the same time, Figure 6(b) shows that the largest deviation from the parabolic behavior (straight line) was measured for the sample exposed to 10^{-5} atm O$_2$. This result is confirmed by the continuous decrease of k_p^i with time (Figure 3(a)), suggesting that the transient stage extends up to about 4.5 hours of exposure with a competitive θ/α growth taking place from the beginning of the exposure, and/or an α-Al$_2$O$_3$ lateral grain growth of the existing α-Al$_2$O$_3$ is occurring at the same time as was proposed in Reference 17. The first conclusion is supported by the presence of residual needle-like microstructure of metastable θ-Al$_2$O$_3$ after 5 hours of oxidation (see Figure 8). Meanwhile, the sample oxidized in 0.21 atm O$_2$ should exhibit at least three different regimes of transformation based on Figure 3(b). Regime I $(0 < t < 2$ hours**)** is where θ-Al$_2$O$_3$ controls the oxidation kinetics. This is followed by a transient regime, region II $(2 < t < 4$ hours) where a competitive growth between θ- and α-Al$_2$O$_3$ occurs and finally a regime III $(t > 4$ hours) in which α-Al$_2$O$_3$ is the controlling phase.

D. *Oxygen Consumption Analysis*

In order to further the above discussion and to highlight the effect of a low p_{O_2} has on the oxidation kinetics of β-(Ni,Pt)Al coatings, a comparison with data available in the literature for oxidation of similar conditions is presented in the following. Figure 9 shows dm_O/dt *vs* t curves for the samples oxidized in 10^{-5} atm O$_2$ (black curves) and 0.21 atm O$_2$ (blue curves) at 1273 K, 1323 K, and 1423 K (1000 °C, 1050 °C, and 1150 °C), along with the comparable curves for θ-Al$_2$O$_3$ and α-Al$_2$O$_3$ based on the oxidation data reported by Brumm and Grabke (red curves) for NiAl alloys oxidized in an He-O$_2$ mix with a $p_{O_2} = 0.13$ atm O$_2$.[21] The k_p values reported in the literature were used to calculate their corresponding dm_O/dt curves using:

$$J_O = \frac{1}{2}\sqrt{\frac{k_p}{t}} = \frac{d(m_O)}{dt} \quad (\text{mg O/cm}^2\,\text{s}) \qquad [11]$$

Based on this comparison and the previous discussion, the following conclusions can be drawn. At 1273 K

(1000 °C), θ-Al$_2$O$_3$ is the phase that controls the oxidation behavior of β-(Ni,Pt)Al independently of the p_{O_2} used in the present work. A good agreement between the sample oxidized in dry air and the Brumm and Grabke data is observed. Taking this into account, it can also be concluded that the slight shift observed for the sample oxidized in 10^{-5} atm O$_2$ is a result of the decrease in θ-Al$_2$O$_3$ growth rate due to a reduction in oxygen potential at the Al$_2$O$_3$/gas interface (Eq. [6]).

At 1323 K (1050 °C), the sample treated in 0.21 atm O$_2$ shows a pure θ-Al$_2$O$_3$ growth below 1 hours of oxidation followed by a transient stage. Similar to the observations at 1273 K (1000 °C), results showed a reduction of the θ-Al$_2$O$_3$ growth rate at 1323 K (1050 °C) in a low p_{O_2}. However, for $t > 3.5$ hours the instantaneous mass-gain rate for the sample oxidized in 0.21 atm O$_2$ became slower. This result supports the faster nucleation observed in 0.21 atm O$_2$ by PSLS.

At 1423 K (1150 °C), θ-Al$_2$O$_3$ is not stable and nucleation of α-Al$_2$O$_3$ occurs from the very early stages of oxidation (first minutes), reaching an α-Al$_2$O$_3$ controlling regime just after about 4.5 hours for the sample oxidized in 0.21 atm O$_2$. Deviations of dm_O/dt values with respect to those expected for α-Al$_2$O$_3$ based the reported data can be explain due to the different compared systems. However, for the sample oxidized in low p_{O_2} a deviation from the expected oxygen consumption rate is observed after about 45 minutes of exposure. This result seems to be at variance with the assumption that α-Al$_2$O$_3$ growth is independent of the external p_{O_2}. However, the observed deviation can be attributed to two different phenomena: (1) the TGO is not a pure n-type semiconductor and a p-type to n-type transition takes place near to the metal/scale interface, as was proposed by Nicolas-Chaubet *et al.*[45] and Heuer *et al.*[22] and (2) the continuous lateral growth of the α-Al$_2$O$_3$ grains is significant enough affect the oxygen diffusion during this period.

With the aim to better understand the gas-supply control effect on competitive growth between θ- and α-Al$_2$O$_3$ during the early stages of oxidation, a basic approach to calculate the flux of oxygen to a flat surface from a gas flowing parallel to it was carried out based on the theory of mass transfer in dilute gases.[46] The present analysis assumed that the working gas contains only one reactive species to promote the sample oxidation. In our case, once the test temperature was reached
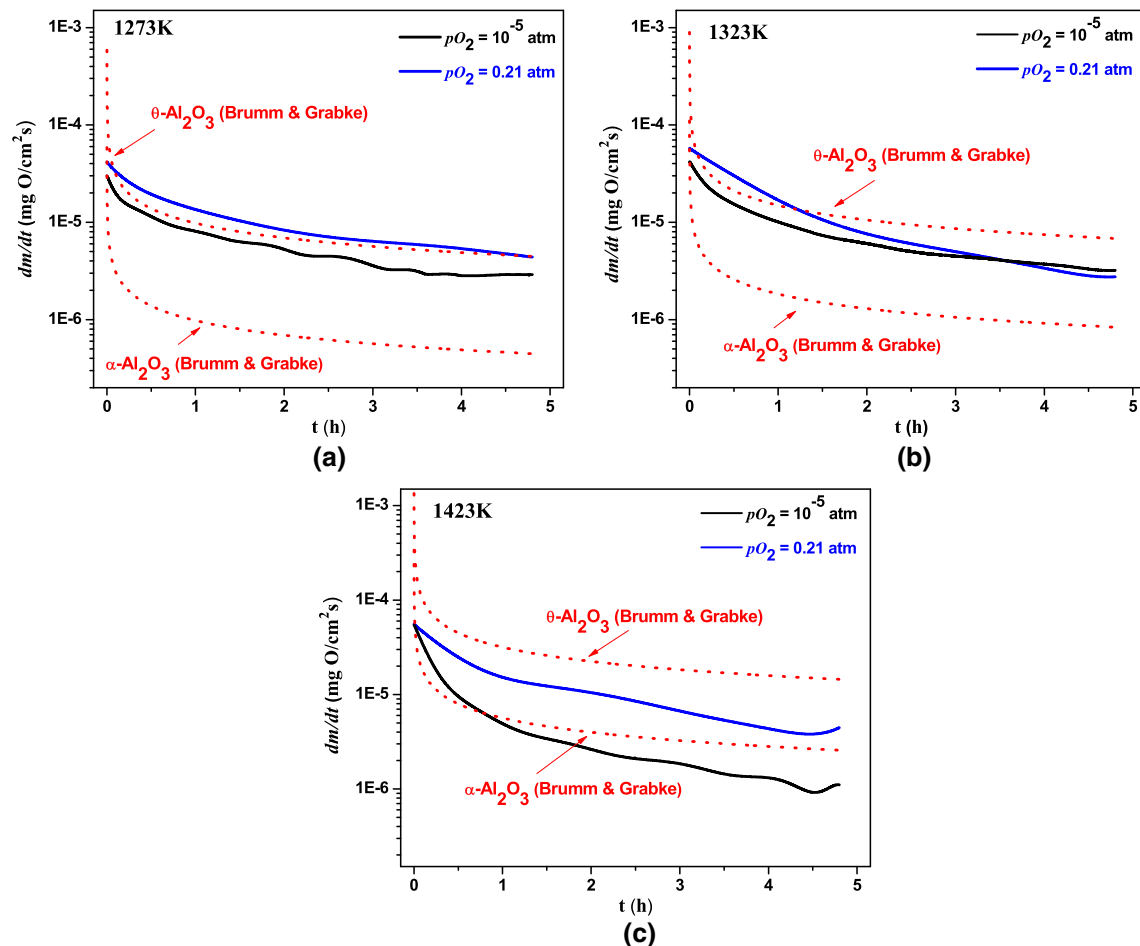
Fig. 9—Comparison of the dm_O/dt vs t curves for as-aluminized samples with Brumm and Grabke data for a NiAl alloy: (a) 1273 K (1000 °C), (b) 1323 K (1050 °C), and (c) 1423 K (1150 °C).

in the furnace chamber, the vacuum was broken, the working gas flowed past the β-(Ni,Pt)Al BC samples and oxygen molecules (the reactive species) transferred from the bulk gas through a boundary layer to the sample-gas interface by diffusion and convection phenomena.[46] Once the oxygen molecules reached the sample surface, the reaction between the Al and O_2 took place to form an alumina scale according to the reaction:

$$2Al(s) + 1.5O_2(g) \rightarrow Al_2O_3(s). \quad [12]$$
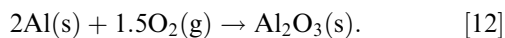
The oxygen flux, J_O^*, is given by

$$J_O^* = 32 \frac{k_m}{RT}(p_{O_2}'' - p_{O_2}')(\text{mg O/cm}^2 \text{ s}), \quad [13]$$

where k_m is mass-transfer coefficient, T absolute temperature, R the universal gas constant, p_{O_2}'' and p_{O_2}' represents the oxygen partial pressure at the working gas-oxide scale and metal-oxide scale interfaces respectively. Two working gas mixtures, p_{O_2}'', were used in the present study. Assuming that p_{O_2}' can be neglected since the oxygen partial pressure at this interface should be defined by the dissociation partial pressure of the alumina, 10^{-40} to 10^{-29} atm, from 1173 K to 1473 K (900 °C to 1200 °C) respectively. As assumed earlier, p_{O_2}' can be neglected. Details of the J_O^* calculations used in this study can be found in the Appendix.

It is generally found that during the very early stages of oxidation of Ni-Al and Ni-Pt-Al alloys, the alumina scale is mainly controlled by the growth of metastable phases (i.e., undoped γ- and/or θ-Al_2O_3 phases) via outward Al diffusion.[37–39] Based on the p-type nature of metastable phases of alumina, an external p_{O_2} can be used to stifle their growth rate as has been showed previously, allowing that the stable α-Al_2O_3 (mainly an n-type oxide) nucleate and grow more freely.

The flux of oxygen available in the working gas at 10^{-5} atm (horizontal green lines) and 0.21 atm O_2 (horizontal orange lines) used in this study are plotted in Figure 10 with the dm_O/dt vs t curves from Figure 9. It is this flux that sustains the growth of the TGO for a given oxygen partial pressure. The flux of oxygen available in the Brumm and Grabke experiments were not been estimated, but it should be on the order of 10^{-2} mg O/cm^2 s.

From Figure 10 it is seen that 0.21 atm O_2 offers enough oxygen for the growth rate of θ-Al_2O_3 to be unaffected: whereas at 10^{-5} atm O_2, the oxygen flux seems to be underestimated at least 30 times with respect to minimum oxygen flux to sustain the observed oxygen
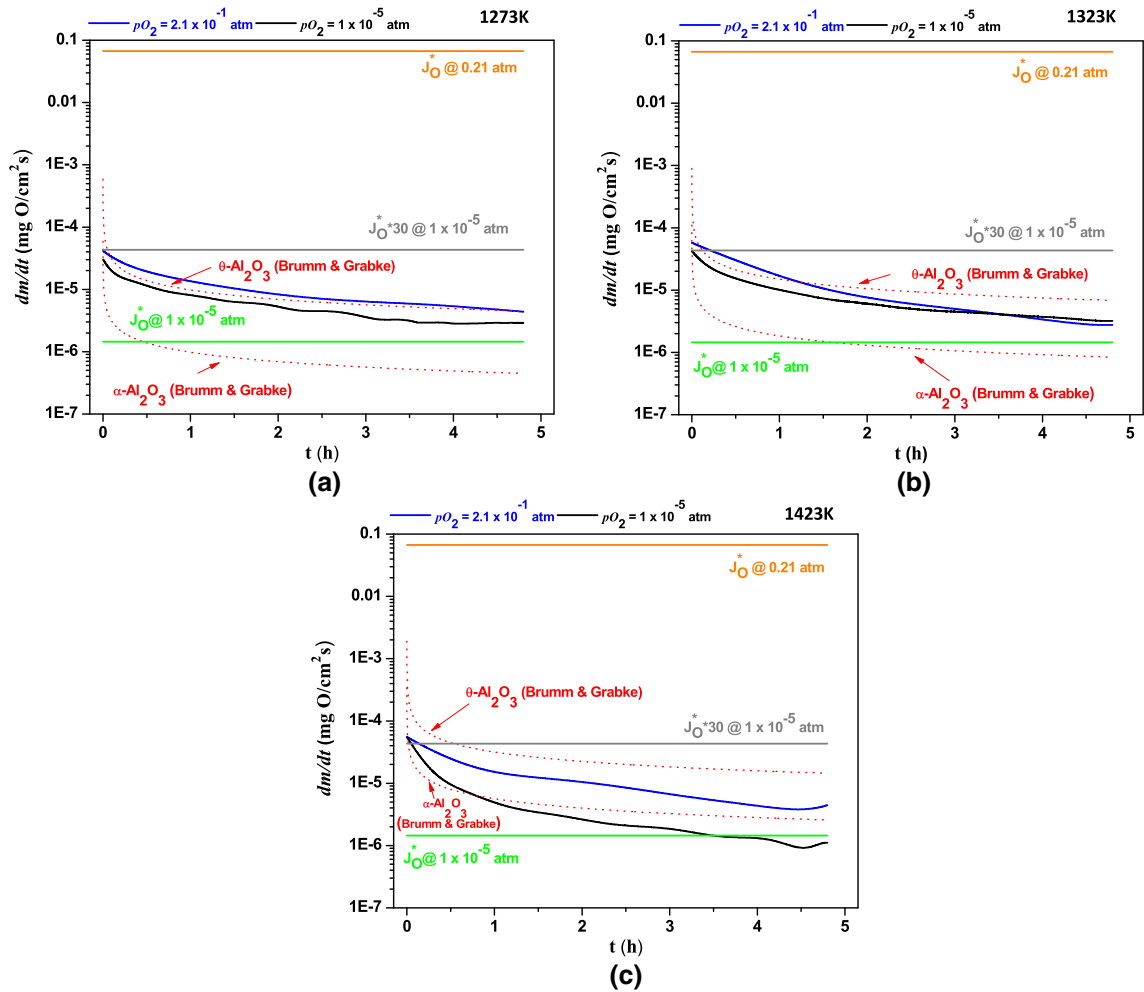
Fig. 10—Comparison of the dm_O/dt vs t curves for as-aluminized samples with the available flux of oxygen during oxidation experiments for the different oxygen partial pressures used. (*a*) 1273 K (1000 °C), (*b*) 1323 K (1050 °C), and (*c*) 1423 K (1150 °C). Red dashed curves refer to Brumm and Grabke data for a NiAl alloy (Color figure online).

consumption rates. A recent publication of Næss *et al.*[47] showed that the classical theory for an uncon-strained flow over a flat plate can lead to an underes-timate the mass transfer coefficient when the velocity profile is not accurately predicted by the boundary layer theory. Deviations of this theory can be expected, for instance, when the boundary layer thickness is signifi-cant compare with the cross section of the experimental setup. A comparison of the setup used by Næss and the one used in this work suggests that we can expect similar or even higher (3 to 7 times higher) deviations. How-ever, the observed deviations in our case are still too high (at least 30 times) to be explained only by this effect.

A further cause for the deviation may be related to the assumption of invariant surface area during the TGA analysis. Traditionally, the surface area of a sample to be used during TGA analysis is estimated based on macroscopic dimensions (length, width and height). However, two additional contributions to the real surface area are missing in this approximation: (1) the surface roughness of the sample and (2) the dynamic

surface area due to TGO microstructure. The real sample surface area is changing with time and temper-ature. It is well known that the metastable γ-Al$_2$O$_3$ and/ or θ-Al$_2$O$_3$ show a platelet-like and/or needle-like morphology. In order to illustrated the above descrip-tion, a surface view of the morphology of the samples oxidized for 5 hours and low p_{O_2} (10^{-5} atm) from 1273 K to 1423 K (1000 °C to 1150 °C) is shown in Figure 11. Based on this figure, it can be seen that the assumption of a flat and homogeneous surface for the kinetic calculations is not valid and clearly underesti-mates the dynamic and heterogeneous surface area.

V. CONCLUSIONS

1. Low oxygen partial pressure conditions suppress the θ-Al$_2$O$_3$ growth in accordance with the theory proposed by Wagner for *p*-type oxide base on the following relation

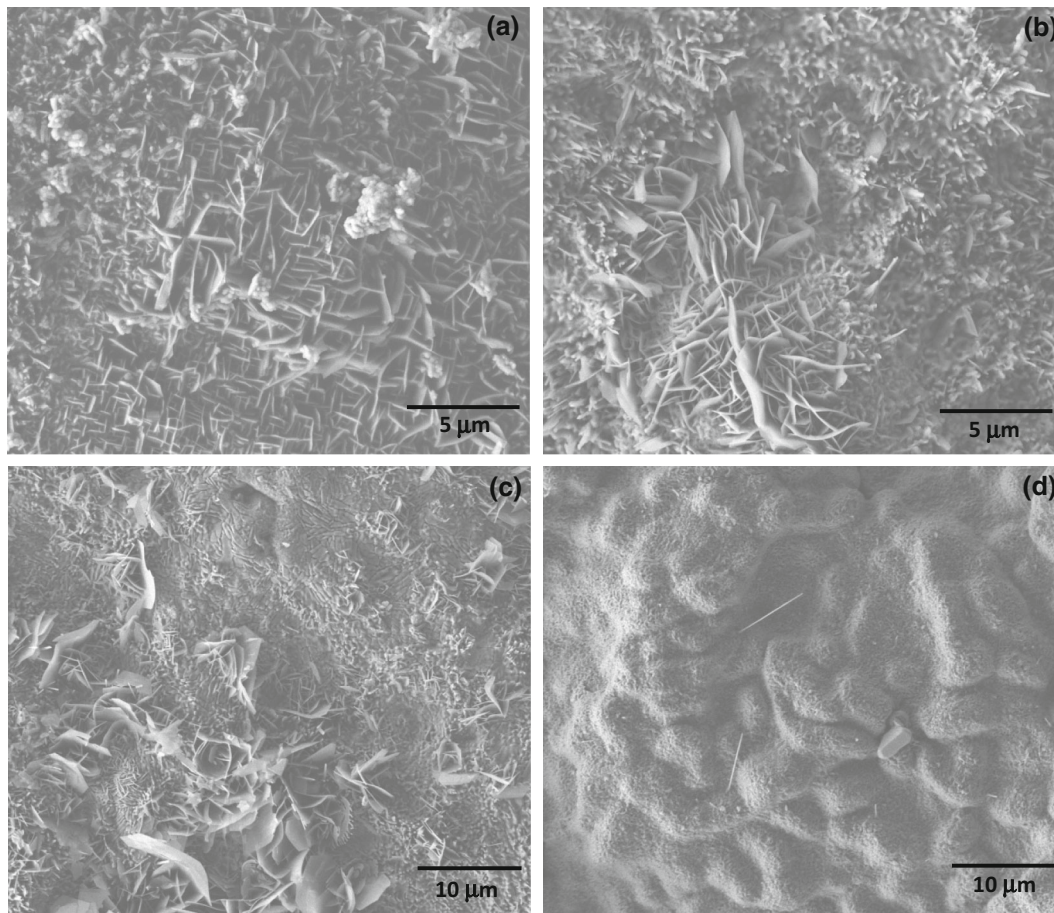$$k_{p\theta} \propto p_{O_2}^{3/16}$$

Fig. 11—Surface microstructure of samples treated for 5 h with a $p_{O_2} = 1 \times 10^{-5}$ atm at: (a) 1273 K (1000 °C), (b) 1323 K (1050 °C), (c) 1373 K (1100 °C), and (d) 1423 K (1150 °C).

Therefore, the shift observed for the parabolic rate constants (after 5 hours of oxidation) to lower values from 1173 K to 1323 K (900 °C to 1050 °C) at a $p_{O_2} = 1 \times 10^{-5}$ atm with respect to the θ-Al$_2$O$_3$ line reported by Brumm and Grabke[21] is mainly a consequence of this inhibition and not to the beginning of transient stage regime.

2. A faster θ-Al$_2$O$_3 \rightarrow \alpha$-Al$_2$O$_3$ transformation was observed from the as-aluminized β-(Ni,Pt)Al BC systems oxidized in dry air in comparison the samples oxidized at a $p_{O_2} = 10^{-5}$ atm from 1273 K to 1473 K (1000 °C to 1200 °C).

3. The macroscopic surface area using during the TGA analysis is significantly underestimated the dynamic real surface area during an oxidation test (about 25 times in our case). This underestimation should be take into account especially when a gas supply control analysis is conducted.

APPENDIX

The oxygen flux, J_O^*, is given by

$$J_O^* = 32 \frac{k_m}{RT}\left(p_{O_2}'' - p_{O_2}'\right) (\text{mg O/cm}^2\,\text{s}), \qquad [A1]$$

where k_m is mass-transfer coefficient, T absolute temperature, and R the universal gas constant. Two working gas mixtures, p_{O_2}'', were used in the present study. As assumed earlier, p_{O_2}' can be neglected. A value of k_m can be evaluated using:

$$k_m = 0.664 \left(\frac{D_{AB}^4}{v}\right)^{\frac{1}{6}} \left(\frac{v_l}{l}\right)^{1/2} (\text{cm/s}), \qquad [A2]$$

where D_{AB} is the diffusion coefficient in an A–B binary gas, v the kinematic viscosity, v_l the linear velocity of the gas and l the length of the surface parallel to gas flow (1.8 cm for all samples). D_{AB} and v values were estimated using the kinetic theory of gases, using the Chapman–Enskog formulation and the gas molecular interaction parameters shown in Table AI.[46]

Table AI. Gas Molecular Interaction Parameters[46]

Species	σ (Å)	ε/k (K)	M (g/mol)
O_2	3.433	113	32.00
N_2	3.667	99.8	28.01
Ar	3.432	122.4	39.95
Air	3.617	97	28.97

Table AII. Mass-Transfer Parameters for O_2 in Ar at a $p_{O_2} = 1 \times 10^{-5}$ atm

T [K (°C)]	D_{AB} (cm²/s)	v (cm²/s)	$0.664(D_{AB}^4/v)^{1/6}$ (cm/s$^{1/2}$)	$(v_l/l)^{1/2}$ (s$^{1/2}$)	k_m (cm/s)	J_O^* (mg O/cm² s)
1273 (1000)	2.33	1.29	1.12	0.605	0.65	1.98×10^{-6}
1323 (1050)	2.48	1.39	1.15	0.629	0.68	2.01×10^{-6}
1373 (1100)	2.64	1.50	1.19	0.653	0.71	2.03×10^{-6}
1423 (1150)	2.80	1.60	1.22	0.676	0.75	2.05×10^{-6}

Table AIII. Mass-Transfer Parameters for O_2 in N_2 at a $p_{O_2} = 0.21$ atm

T [K (°C)]	D_{AB} (cm²/s)	v (cm²/s)	$0.664(D_{AB}^4/v)^{1/6}$ (cm/s$^{1/2}$)	$(v_l/l)^{1/2}$ (s$^{1/2}$)	k_m (cm/s)	J_O^* (mg O/cm² s)
1273 (1000)	2.41	1.18	1.16	0.58	0.67	6.48×10^{-2}
1323 (1050)	2.57	1.27	1.20	0.59	0.71	6.54×10^{-2}
1373 (1100)	2.73	1.37	1.23	0.60	0.74	6.61×10^{-2}
1423 (1150)	2.90	1.47	1.27	0.61	0.78	6.68×10^{-2}

Accordingly, D_{AB} is defined as

$$D_{AB} = \frac{1.858 \times 10^{-3}\sqrt{T^3\left(\frac{1}{M_A} + \frac{1}{M_B}\right)}}{P\sigma_{AB}^2\Omega_{D,AB}} \ (cm^2/s), \quad [A3]$$

where

$$\sigma_{AB} = \frac{\sigma_A + \sigma_B}{2} \ (\text{Å}) \quad [A4]$$

$$\Omega_{D,AB} = \frac{1.06036}{T^{*0.1561}} + \frac{0.193}{\exp(0.47635T^*)} + \frac{1.03587}{\exp(1.52996T^*)}$$
$$+ \frac{1.76474}{\exp(3.89411T^*)}$$
$$[A5]$$

$$\frac{\varepsilon_{AB}}{k} = \frac{\sqrt{\varepsilon_A\varepsilon_B}}{k} \ (K^{-1}) \quad [A6]$$

$$T^* = \frac{kT}{\varepsilon_{AB}} \quad [A7]$$

Here, σ is the collision diameter, Ω_D the diffusion collision integral, ε the characteristic energy of interaction (used in the Lennard–Jones potential), M the molecular weight, k Boltzman's constant and P the system pressure (set to 1 atm during TGA analysis). The subscripts A and B represent the gaseous species considered during the interactions.

Meanwhile, v is given by

$$v = \frac{\eta}{\rho} \ (cm^2/s), \quad [A8]$$

where η and ρ are the average values of viscosity and density of the species in the working gas, respectively. η is given by

$$\eta_i = 2.6693 \times 10^{-5} \frac{\sqrt{M_i T}}{\sigma\Omega_\eta} \ (\text{poise}) \quad [A9]$$

$$\eta_{mix} = \sum_{\alpha=1}^{N} \frac{x_\alpha \eta_\alpha}{\sum_\beta x_\beta \phi_{\alpha\beta}} \ (\text{poise}) \quad [A10]$$

$$\Omega_\eta = \frac{1.16145}{T^{*0.14874}} + \frac{0.52487}{\exp(0.7732T^*)} + \frac{2.16178}{\exp(2.43787T^*)}$$
$$[A11]$$

$$\phi_{\alpha\beta} = \frac{1}{\sqrt{8}}\left(1 + \frac{M_\alpha}{M_\beta}\right)^{-1/2}\left[1 + \left(\frac{\eta_\alpha}{\eta_\beta}\right)^{1/2}\left(\frac{M_\alpha}{M_\beta}\right)^{1/4}\right]^2,$$
$$[A12]$$

where η_i is the viscosity of the pure species i, η_{mix} the viscosity of mixed species and Ω_η the viscosity collision integral. The mass-transfer parameters for the different oxidizing conditions used in this work were calculated from Eqs. [A1] to [A12] and are tabulated in Tables AII and AIII.

REFERENCES

1. J.R. Nicholls: *MRS Bull.*, 2003, vol. 28 (9), pp. 659–70.
2. D.R. Clarke and C.G. Levi: *Annu. Rev. Mater. Res.*, 2003, vol. 33, pp. 383–417.
3. R.C. Reed: *The Superalloys Fundamentals and Applications*, Cambridge University Press, Cambridge, ISBN 978-0-511-24546-6, 2006, p. 283.
4. J.R. Nicholls: *JOM*, 2000, vol. 52 (1), pp. 28–35.
5. S. Bose: *High Temperature Coatings*, Elsevier Science & Technology Books, New York, ISBN 0750682523, 2007, pp. 155–232.
6. G.W. Goward and D.H. Boone: *Oxid. Met.*, 1971, vol. 3, pp. 475–95.
7. R. Streiff, O. Cerclier, and D.H. Boone: *Surf. Coat. Technol.*, 1987, vol. 32, pp. 111–26.
8. B.M. Warnes and D.C. Punola: *Surf. Coat. Technol.*, 1997, vols. 94–95, pp. 1–6.
9. B.M. Warnes: *Surf. Coat. Technol.*, 2001, vols. 146–147, pp. 7–12.
10. B.A. Nagaraj, W.B. Connor, R.W. Jendrix, D.J. Wortman, and L.W. Plemmons: US Patent 5,427,866, 1995.
11. S. Hayashi and B. Gleeson: *Oxid. Met.*, 2009, vol. 71 (1–2), pp. 5–19.
12. A.G. Evans, D.R. Clarke, and C.G. Levi: *J. Eur. Ceram. Soc.*, 2008, vol. 28 (7), pp. 1405–19.
13. W. Gao and Z. Li: *Developments in High-Temperature Corrosion and Protection of Materials*, Woodhead Publishing, Cambridge, ISBN 978-1-84569-425-8, 2008, pp. 476–89.
14. A.G. Evans, D.R. Mumm, J.W. Hutchinson, G.H. Meier, and F.S. Pettit: *Prog. Mater Sci.*, 2001, vol. 46, pp. 505–53.
15. D.R. Clarke and F. Adar: *J. Am. Ceram. Soc.*, 1982, vol. 65 (6), pp. 284–88.
16. D.M. Lipkin and D.R. Clarke: *Oxid. Met.*, 1996, vol. 45 (3–4), pp. 267–80.
17. I. Spitsberg and K. More: *Mater. Sci. Eng. A*, 2006, vol. 417 (1–2), pp. 322–33.
18. V.K. Tolpygo and D.R. Clarke: *Surf. Coat. Technol.*, 2005, vol. 200 (5–6), pp. 1276–81.
19. L.M. He, Y.F. Su, L.F. Allard, M.J. Lance, and W.Y. Lee: *Metall. Mater. Trans. A*, 2004, vol. 35A, pp. 1113–24.
20. G.C. Rybicki and J.L. Smialek: *Oxid. Met.*, 1989, vol. 31 (3–4), pp. 275–304.
21. M.W. Brumm and H.J. Grabke: *Corros. Sci.*, 1992, vol. 33 (11), pp. 1677–90.
22. A.H. Heuer, D.B. Hovis, J.L. Smialek, and B. Gleeson: *J. Am. Ceram. Soc.*, 2011, vol. 94 (S1), pp. s146–53.
23. Y. Zhang, W.Y. Lee, J.A. Haynes, I.G. Wright, B.A. Pint, K.M. Cooley, and P.K. Liaw: *Metall. Mater. Trans. A*, 1999, vol. 30A, pp. 2679–87.
24. M. Matsumoto, T. Kato, K. Hayakawa, N. Yamaguchi, S. Kitoaka, and H. Matsubara: *Surf. Coat. Technol.*, 2008, vol. 202 (12), pp. 2743–248.
25. A. Hesnawi, L. Hefei, Z. Zhaohui, G. Shengkai, and X. Huibin: *Surf. Coat. Technol.*, 2007, vol. 201 (15), pp. 6793–96.
26. D. Monceau, K. Bouhanek, R. Peraldi, A. Malie, and B. Pieraggi: *J. Mater. Res.*, 2000, vol. 15 (3), pp. 665–75.
27. Y. Cadoret, D. Monceau, M.P. Bacos, P. Jasso, V. Maurice, and P. Marcus: *Oxid. Met.*, 2005, vol. 64 (3–4), pp. 185–205.
28. B. Baufeld and U. Shulz: *Surf. Coat. Technol.*, 2006, vol. 201 (6), pp. 2667–75.
29. J.M. Alvarado-Orozco: Ph.D. Thesis, Mexico, 2011.
30. Q. Ma and D.R. Clarke: *J. Am. Ceram. Soc.*, 1993, vol. 76 (6), pp. 1433–40.
31. D.M. Lipkin, H. Schaffer, F. Adar, and D.R. Clarke: *Appl. Phys. Lett.*, 1997, vol. 70 (19), pp. 2550–52.
32. X. Lu, S. Venugopalan, H. Kim, M. Grimsditch, S. Rodriguez, and A.K. Ramdas: *Phys. Rev. B*, 2009, vol. 79(23), pp. 235204-1–4-7.
33. J.M. Alvarado-Orozco, R. Morales-Estrella, M.S. Boldrick, J.L. Ortiz-Merino, D.G. Konitzer, G. Trápaga-Martínez, and J. Muñoz-Saldaña: *Oxid. Met.*, 2012, vol. 78, pp. 269–84.
34. T.G. Tammann: *Z. Anorg. Allgem. Chem.*, 1920, vol. 111 (1), pp. 78–89.
35. C. Wagner: *J. Electrochem. Soc.*, 1952, vol. 99 (10), pp. 369–80.
36. D. Monceau and B. Pieraggi: *Oxid. Met.*, 1998, vol. 50 (5–6), p. 477493.
37. J. Jedlinski and G. Borchardt: *Solid State Ionics*, 1991, vol. 50 (1–2), pp. 67–74.
38. J. Doychak, J.L. Smialek, and T.E. Mitchell: *Metall. Trans. A*, 1989, vol. 20A, pp. 499–518.
39. B.A. Pint, J.R. Martin, and L.W. Hobbs: *Solid State Ion.*, 1995, vol. 78 (1–2), pp. 99–107.
40. F.A. Kröger and H.J. Vink: in *Solid State Physics: Advances and Applications*, vol. 3, F. Seitz, and D. Turnbull, eds., Academic Press, New York, 1956, p. 307.
41. C. Wagner: *Z. Phys. Chem.*, 1933, vol. B21, pp. 25–30.
42. R.G. Bagwell, G.L. Messing, and P.R. Howell: *J. Mater. Sci.*, 2001, vol. 36 (7), pp. 1833–41.
43. M.W. Brumm and H.J. Grabke: *Corros. Sci.*, 1993, vol. 34 (4), pp. 547–553, 555–561.
44. B.A. Pint: *Oxid. Met.*, 1997, vol. 48 (3–4), pp. 303–28.
45. D. Nicolas-Chaubet, A.M. Huntz, and F. Millot: *J. Mater. Sci.*, 1991, vol. 26 (22), pp. 6119–26.
46. R.B. Bird, W.E. Stewart, and E.N. Ligthfoot: *Transport Phenomena*, 2nd ed., Wiley, New York, 2002, p. 866.
47. M.K. Næss, D.J. Young, J. Zhang, J.E. Olsen, and G. Tranell: *Oxid. Met.*, 2012, vol. 78 (5–6), pp. 363–76.